Mechanical Characterisation of Woven Pneumatic Active Textile

Ruby Marshall[1], Jean-Baptiste R. G. Souppez[2], Mariya Khan[2], Ignazio Maria Viola[3], Hiroyuki Nabae[4], Koichi Suzumori[4], Adam A. Stokes[1] and Francesco Giorgio-Serchi[1]

***Abstract*—Active textiles have shown promising applications in soft robotics owing to their tunable stiffness and design flexibility. Given the breadth of the design space for planar and spatial arrangements of these woven structures, a rigorous and generalizable characterisation of these systems is not yet available. In order to characterize the response of a stereotypical woven pattern to actuation, we undertake a parametric study of plain weave active fabrics and characterise their mechanical properties in accordance with the relevant ISO standards for varying muscle densities and both monotonically increasing/decreasing pressures. Tensile and flexural tests were undertaken on five plain weave samples made of a nylon 6 (polyamide) warp and EM20 McKibben S-muscle weft, for input pressures ranging from 0.00 MPa to 0.60 MPa, at three muscle densities, namely 100 $\mathbf{m}^{-1}$, 74.26 $\mathbf{m}^{-1}$ and 47.62 $\mathbf{m}^{-1}$. Contrary to intuition, we find that a lower muscle density has a more prominent impact on the thickness, but a significantly lesser one on length, highlighting a critical dependency on the relative orientation among the loading, the passive textile and the muscle filaments. Hysteretic behaviour as large as 10% of the longitudinal contraction is observed on individual filaments and woven textiles, and its onset is identified in the shear between the rubber tube and the outer sleeve of the artificial muscle. Hysteresis is shown to be muscle density-dependent and responsible for a strongly asymmetrical response upon different pressure inputs. These findings provide new insights into the mechanical properties of active textiles with tunable stiffness, and may contribute to future developments in wearable technologies and biomedical devices.**

***Index Terms*—Wearable Robotics; Soft Robot Materials and Design; Hydraulic/Pneumatic Actuators**

I. Introduction

With the increased pervasiveness of robotic technology into our society, novel actuators are being developed which address the pressing need of facilitating human-robot physical interaction. Textile actuators [1] offer unprecedented potential in easing the adoption of robotics technology in our everyday life to the point of including mechatronic devices in our dressing habits. Indeed, wearable technologies have lately received widespread interest and are forecast to soon represent a conspicuous share of the biomedical, entertainment and fashion markets [2]. The prospect of seamlessly incorporating health-assistive devices in our garments, or cooperating with inherently safe robotics companions thanks to their textile-based structure is, for the first time, made tangible by the recent advancements in active textile technology, with examples shown in Fig. 1.

Fig. 1. Examples of woven active textile: (a) a stiffness-controllable wrist band, (b) a stiffness-tunable elbow compression sleeve and (c) knee and foot soft prosthetic support.

Active textiles encompass flexible sheets manufactured with fiber-like elements capable of undergoing deformation when subject to electromechanical forcing from shape memory alloys and polymers, electroactive polymers and other types of actuators, as reviewed by [3]–[5]. While fluidic actuation has been sparsely associated with active textile technology due to the bulkiness and rigidity of the constituent pneumatic unit, recent work from [6] demonstrates the asset of filament-like, thin McKibben muscles for the development of fluidic textiles. The work of [6] and [7], while overlooking an in-depth mechanical parametrisation of the textile, shows how to exploit the high power density and short response times of a fluidic drive with the design flexibility of textiles to

Manuscript received: November, 18, 2022; Revised February, 24, 2023; Accepted March, 18, 2023.

This paper was recommended for publication by Editor Jee-Hwan Ryu upon evaluation of the Associate Editor and Reviewers' comments.

[1]R. Marshall, A. Stokes and F. Giorgio-Serchi are with University of Edinburgh, School of Engineering, Integrated Micro and Nano Systems Institute, Edinburgh, UK ruby.marshall@ed.ac.uk, adam.stokes@ed.ac.uk, f.giorgio-serchi@ed.ac.uk

[2]J.B. Souppez and M. Khan are with Aston University, College of Engineering and Physical Sciences, School of Engineering and Technology, Department of Mechanical, Biomedical and Design Engineering, Birmingham, UK j.souppez@aston.ac.uk, 190055091@aston.ac.uk

[3]I.M. Viola is University of Edinburgh, School of Engineering, Institute of Energy Systems, Edinburgh, UK i.m.viola@ed.ac.uk

[4]N. Hiroyki and K. Suzumori are with Tokyo Institute of Technology, Department of Mechanical Engineering, Tokyo, Japan nabae.h.aa@m.titech.ac.jp, suzumori.k.aa@m.titech.ac.jp

Digital Object Identifier (DOI): see top of this page.

realise high performance active fabrics for wearable, haptic and biomedical applications, [8]–[11].

The filament-like nature of the thin McKibben muscles lends itself to their implementation in the active textile multifilament assemblies and woven patterns. A parallel arrangement of filaments offers a tensile actuation force that scales with fibre count, highlighting a promising parallelism with biological muscle bundles. Woven textile assemblies, on the other hand, provide a mean to generate asymmetric and non-homogenous stiffening of the fabric, thus opening a boundless design space for developing garments with the capability to undergo multi degree of freedom controlled deformations. It is this inherent flexibility in the design and weaving of the active textile that lends itself to applications ranging from surgical robotics, wearable devices and health technology. Social robotics, including sensory devices and companion robots, will benefit from the range of potential applied force that woven active fabrics can exert to satisfy the delicate human-centred social robotic design requirements with respect to tactile sensory input and individual psychology [12]–[14]. Similarly, active textiles enable the ability to fine-tune the transition across gradients of rigidity for the design of soft exo-suits [15] providing static support while not impeding movement and their garment-like nature makes them ideal for implementation in soft rehabilitation equipment [16] and even wearable cardiac ventricular assist devices [17].

However, owing to the lack of a systematic characterization of the mechanical properties of woven active textiles, the exploration of their design space has so far been largely empirical, posing limitation to their widespread adoption in applicative scenarios. In this work we address the need for a rigorous parametric identification of woven pneumatic active textiles by undertaking mechanical characterization of a stereotypical woven patterns with different muscle density for monotonically increasing and monotonically decreasing pressures. The tests are performed in accordance with standardized ISO protocols to ensure their relevance, accuracy and repeatability.

The remainder of the paper is structured as follows. Section II introduces the pneumatic active textile under consideration and its characteristics. Section III presents the experimental setup, protocol and associated uncertainty. Then, the results for the geometrical and mechanical properties are reported in Section IV, with their significance detailed in Section V. Finally, Section VI summarises the main findings.

II. Active textile

The active textile samples manufactured consist of a warp and a weft, combined using a plain weave, as shown in Fig. 2. The warp is lengthwise, i.e. in the direction of the applied tensile load. The weft is defined as normal to the warp. The warp is a nylon 6 (polyamide) line with a $1.50\,\mathrm{mm}$ nominal diameter and a measured dry mass per unit length of $0.78\,\mathrm{g\,m^{-1}}$, or mass per unit surface area of $520.00\,\mathrm{g\,m^{-2}}$. The weft is a pneumatic artificial muscle, namely a thin EM20 McKibben S-muscle, having a nominal outer diameter $D_0 = 3.00\,\mathrm{mm}$ at an input pressure $P = 0.00\,\mathrm{MPa}$ (i.e. uninflated), and a measured dry mass per unit length of $2.44\,\mathrm{g\,m^{-1}}$, or dry mass per unit surface area $813.33\,\mathrm{g\,m^{-2}}$. The outer sleeve is made of 32 spindles of polyethylene terephthalate monofilaments with a $0.16\,\mathrm{mm}$ nominal diameter at a 19° angle. The inner synthetic rubber tube has a $1.8\,\mathrm{mm}$ inner and $2.2\,\mathrm{mm}$ outer diameter [7]. All linear geometric quantities in this paper are the average of three measurements over each individual sample.

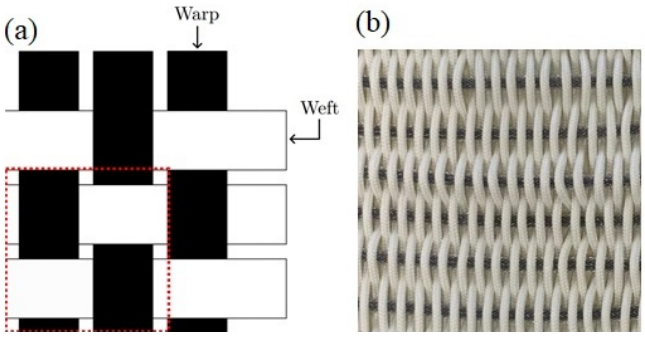

Fig. 2. (a) Schematic of a warp and weft combined in a plain weave pattern with a repeating unit shown in red, and (b) example of plain weave active textile.

In this work, the pneumatic muscle and plain weave adopted are characteristic of the textile designs encountered in soft-robotic applications [7], [18]–[20]. The application of the present mechanical characterization to highly convoluted planar and spatial woven patterns represents an obvious expansion of the current work towards realizing a broader type of controllable actuation such as twist, bend and compression.

We define the muscle density ρ_M as

$$\rho_M = \frac{1}{s_{\mathrm{weft}}\ [\mathrm{m}]} = \frac{n_{\mathrm{weft}}}{L_0\ [\mathrm{m}]}, \tag{1}$$

where s_{weft} is the weft spacing (in meter), i.e. the lengthwise spacing between two wefts. This corresponds to the number of weft per meter warp. The muscle density may also be expressed as the ratio of the number of wefts of the sample, n_{weft}, to the gauge length L_0 (in meter). Three muscle densities are investigated, namely $\rho_M = 100\,\mathrm{m^{-1}}$, $\rho_M = 74.26\,\mathrm{m^{-1}}$ and $\rho_M = 47.62\,\mathrm{m^{-1}}$, respectively identified with sample $S100$, $S74$ and $S48$, depicted in Fig. 3(a). $S100$ is intended to replicate the weft spacing of [7], while $S48$ halves that number of wefts, and $S74$ provides intermediate values to investigate the effect of muscle density.

Prior to testing, each muscle undergoes a warm-up cycle. This consists of an incremental input pressure cycle from $P = 0.00\,\mathrm{MPa}$ to $P = 0.60\,\mathrm{MPa}$ in $0.10\,\mathrm{MPa}$ increments and back to $P = 0.00\,\mathrm{MPa}$ between each increment. Each increment is repeated twice before moving on to the next. This is necessary to ensure that the Mullins effect [21], whereby the cyclic softening of rubber materials varies with the previous maximum supplied pressure, stabilises. This protocol guarantees that any hysteretic behaviour observed in Section IV is uniquely attributed to the friction between the outer sleeve and inner tubing of the muscles [7].

Five samples ($n = 5$) were manufactured, in line with ISO requirements [22], [23]. The woven samples are made of 34 strands for the warp, giving a gauge length $L_0 = 200\,\mathrm{mm}$ at $P = 0.00\,\mathrm{MPa}$ for $S100$, and a width $b = 50\,\mathrm{mm}$. Both

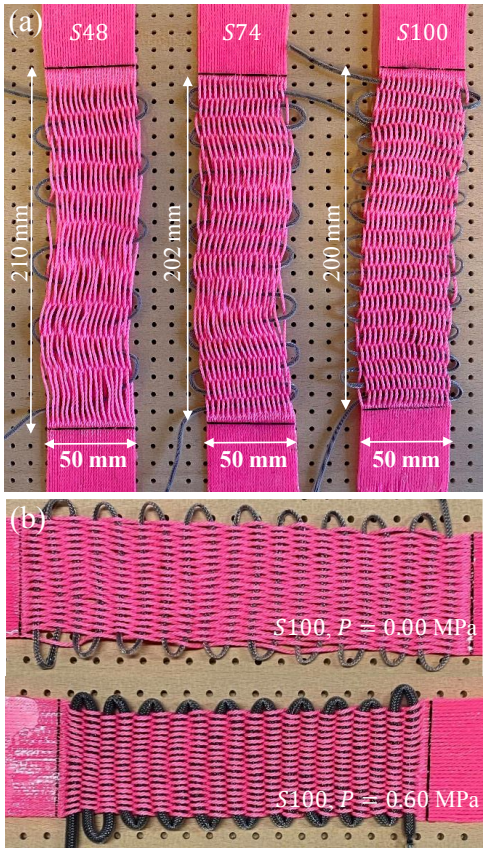

Fig. 3. (a) Test samples (left) $S48$, $\rho_M = 47.62\,\mathrm{m}^{-1}$, 10 wefts for $L_0 = 210\,\mathrm{mm}$, (center) $S74$, $\rho_M = 74.26\,\mathrm{m}^{-1}$, 15 wefts for $L_0 = 202\,\mathrm{mm}$, and (right) $S100$, $\rho_M = 100\,\mathrm{m}^{-1}$, 20 wefts for $L_0 = 200\,\mathrm{mm}$, all at $P = 0.00\,\mathrm{MPa}$. (b) $S100$ at $P = 0.00\,\mathrm{MPa}$ (top) and $P = 0.60\,\mathrm{MPa}$ (bottom).

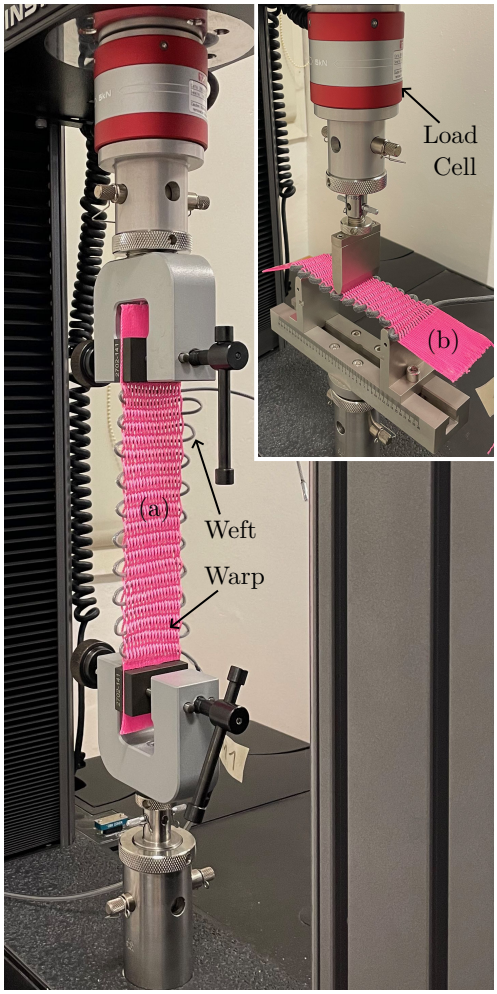

Fig. 4. Experimental setup depicting textile sample $S100$ in (a) tension and (b) flexion (3-point bend).

dimensions are in accordance with the ISO 13934-1:2013 [24] for textiles. The unwoven muscle length employed was $L_M = 1500\,\mathrm{mm}$ for sample $S100$. Note that an unwoven warp length of $215\,\mathrm{mm}$ is necessary to achieve the desired woven gauge length $L_0 = 200\,\mathrm{mm}$ at $P = 0.00\,\mathrm{MPa}$ for $S100$. For $S74$ and $S48$, at $P = 0.00\,\mathrm{MPa}$, the woven gauge length is $202\,\mathrm{mm}$ and $210\,\mathrm{mm}$, respectively, as shown in Fig. 3(a). The longitudinal contraction for $S100$ between $P = 0.00\,\mathrm{MPa}$ and $P = 0.60\,\mathrm{MPa}$ is depicted in in Fig. 3(b). The end tabbing at each lengthwise extremity of the samples is $50\,\mathrm{mm}$ long by $50\,\mathrm{mm}$ wide, and reinforced with epoxy resin.

III. Methods

A. Experimental Setup and Protocol

Experiments were performed on a universal testing machine (Instron 5965 series) at Aston University, employing a 5 kN loadcell (see details of experimental biases in Table I). The apparatus and tensile setup are depicted in Fig. 4(a), and the flexural (3-point bend) setup is shown in Fig. 4(b).

Forces were measured at a sampling rate of $200\,\mathrm{Hz}$. All experiments were conducted within the following ranges for the temperature $17.5\,^{\circ}\mathrm{C} \leq T \leq 25.7\,^{\circ}\mathrm{C}$ and relative humidity $0.305 \leq \varphi \leq 0.535$. For tensile tests, a $1\,\mathrm{N}$ preload is applied at a displacement rate of $10\,\mathrm{mm\,min}^{-1}$. This is intended to remove any slack in the sample before the test starts. The load is then applied at a displacement rate of $1\,\mathrm{mm\,min}^{-1}$ up to a tensile strain $\epsilon = 0.003$, with

$$\epsilon = \frac{\Delta L_0}{L_0} \tag{2}$$

where ΔL_0 and L_0 are the tensile displacement and the gauge length, respectively. The same protocol is applied in flexion, with the exception of the pre-load threshold set at $0.02\,\mathrm{N}$. All experiments are conducted for $\epsilon \leq 0.003$ to ensure that the testing lies outside of the plastic deformation range of the warp, thereby ensuring no loss of properties throughout the test campaign due to excessive strain.

B. Tensile and Flexural Properties

From the measured forces and displacements, tensile and flexural properties are computed as follows, according to the ISO 527-2:2012 [23] and the ISO 178:2019 [22], respectively. First, the strain is ascertained. In tension, the strain ϵ is a function of the gauge length L_0, which varies with the input pressure (see Fig. 6 in Section IV-B). Conversely, the flexural strain reads

$$\epsilon_f = \frac{6wh}{s^2} \tag{3}$$

where h is the thickness of the sample, w is the deflection and s is the span, taken here as constant at $s = 120\,\mathrm{mm}$.

The tensile stress is defined as

$$\sigma = \frac{F}{bh} \tag{4}$$

and the flexural stress as

$$\sigma_f = \frac{3Fs}{2bh^2}. \tag{5}$$

Given the applied force F, it is possible to compute the stresses σ (4) and σ_f (5) for tension and flexion, respectively. Finally, the tensile modulus, also known as the modulus of elasticity, or Young's modulus,

$$E = \frac{\sigma}{\epsilon} \tag{6}$$

and the flexural modulus

$$E_f = \frac{\sigma_f}{\epsilon_f} \tag{7}$$

are computed using the linear least squares method for $0.0005 \leq \epsilon \leq 0.0025$ and $0.0005 \leq \epsilon_f \leq 0.0025$, respectively [22].

C. Uncertainty

The uncertainty U associated with the results is given as the root sum of the precision A and the bias B, such that

$$U = \sqrt{(A^2 + B^2)}, \tag{8}$$

with

$$A = \frac{t_{95}S}{\sqrt{n}}, \tag{9}$$

where $t_{95} = 2.776$ for $n = 5$ at the 95% confidence level [25], and S is the standard deviation of the average results. The experimental bias limits are presented in Table I. Following the above uncertainty estimation commonly applied to composite materials [26], the error bars presented throughout Section IV are used to represent the 95% confidence interval around the data collected.

Force, $B(F)$ [N]	0.00005
Width, $B(b)$ [mm]	0.005
Thickness, $B(h)$ [mm]	0.005
Length, $B(L_0)$ [mm]	0.5
Elongation, $B(\Delta L_0)$ [mm]	0.00005
Span, $B(s)$ [mm]	0.005
Deflection, $B(w)$ [mm]	0.00005

TABLE I
SUMMARY OF THE BIAS LIMITS.

IV. RESULTS

A. Weft Characterisation

The length L and diameter D of the individual, unwoven EM20 S-muscles were measured for monotonically increasing and then monotonically decreasing pressures. This is particularly relevant to robotics actuation to ensure the symmetrical response of an actuator under different duty cycles. The variations in radial expansion and longitudinal contraction are expressed as D/D_0 and L/L_M, and are presented in Fig. 5 and Fig. 6, respectively.

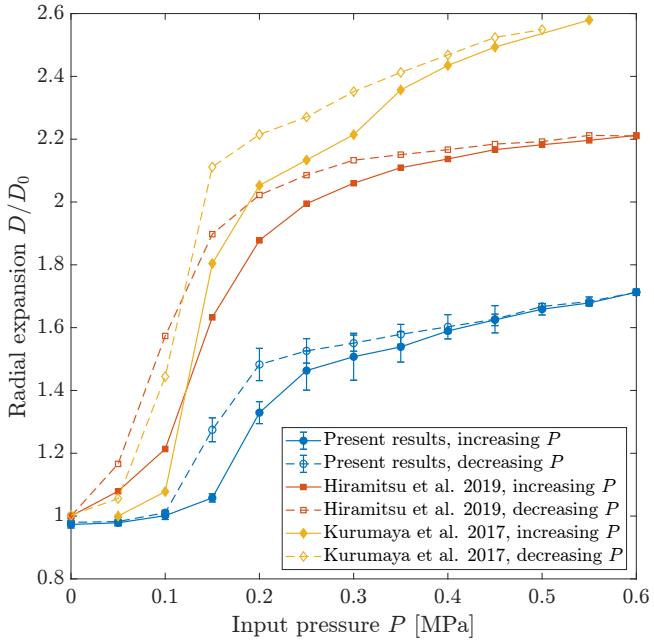

Fig. 5. Radial expansion D/D_0 of unwoven EM20 S-muscles for $0.00\,\mathrm{MPa} \leq P \leq 0.60\,\mathrm{MPa}$, including data from [6] and [7].

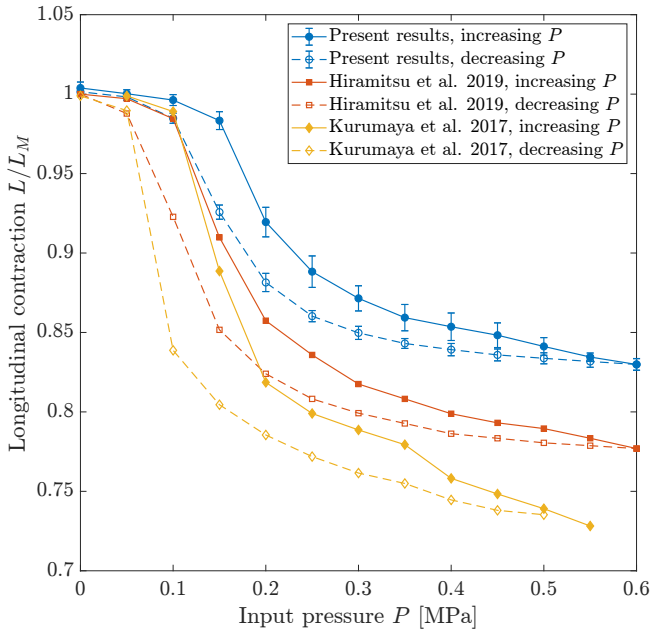

Fig. 6. Longitudinal contraction L/L_M of unwoven EM20 S-muscles for $0.00\,\mathrm{MPa} \leq P \leq 0.60\,\mathrm{MPa}$, including data from [6] and [7].

The results reveal a clear hysteresis for both D/D_0 and L/L_M. The latter, however, occurs over a larger range of input pressure than the former. This observation is consistent with the previously reported results of [7] and [6]. As previously noted in Section II, the muscles were repeatedly pre-loaded up to the maximum pressure to alleviate the Mullins effect. Therefore, the hysteresis is considered to arise from the friction between the rubber tube and the outer sleeve of the artificial

muscle.

The magnitude of the radial expansion and longitudinal contraction appear lesser than reported in other studies [6], [7]. Indeed, in this work, at $P = 0.60\,\text{MPa}$, $D/D_0 = 1.71$ and $L/L_M = 0.83$, whereas [7] reported values of $D/D_0 = 2.21$ and $L/L_M = 0.78$ at $P = 0.60\,\text{MPa}$ on an identical muscle with $L_M = 2500\,\text{mm}$. On the other hand, [6] employed a silicon tube on a muscle with $D_0 = 1.8\,\text{mm}$ and $L_M = 300\,\text{mm}$ up to $P = 0.55\,\text{MPa}$. At this input pressure, $D/D_0 = 2.58$ and $L/L_M = 0.73$.

While different muscles of different length all exhibit a common behaviour, namely a hysteresis between an increasing and decreasing pressure cycle, the magnitude of the radial expansion and longitudinal contraction has been shown to vary significantly. This could be seen as a hurdle to accurately predicting the geometric definition of woven active textiles. As such, characterisation of the effect of input pressure on the thickness and gauge length of plain weave samples is undertaken.

B. Active Textile Characterisation

The thickness h and length L of each of the individual, woven samples were measured to yield the variations in thickness expansion h/h_0 and longitudinal contraction L/L_0, where h_0 and L_0 are the thickness and gauge length at $P = 0.00\,\text{MPa}$, respectively. The results are presented in Fig. 7 for the thickness expansion and Fig. 8 for the longitudinal contraction. Here, we quantify the overall thickness h of the whole woven textile samples, as opposed to the diameter D for the unwoven muscles previously employed in Section IV-A. Similarly, the longitudinal contraction is now based on the sample's gauge length L_0 as opposed to the previously employed muscle length L_M.

The hysteretic behavior of sample $S100$ is consistent with that observed for unwoven muscles in Section IV-A for both h/h_0 and L/L_0. For sample $S74$ and $S48$ the thickness expansion exhibits a similar behaviour to that of $S100$, but with a maximum value at $P = 0.60\,\text{MPa}$ of $h/h_0 = 1.53$ and $h/h_0 = 1.55$, respectively. This compares to $h/h_0 = 1.47$ for $S100$ at the same input pressure. There is, therefore, a reduction in the thickness expansion for increasing muscle density. Moreover, the hysteresis affecting h/h_0 extends to a higher pressure range for decreasing muscle density. Indeed, this is observed up to $P \leq 0.35\,\text{MPa}$ for $S100$, $P \leq 0.40\,\text{MPa}$ for $S74$, and $P \leq 0.45\,\text{MPa}$ for $S48$.

A radically different behaviour is exhibited for the longitudinal contraction, which is more pronounced for increasing muscle density. This yields $L/L_0 = 0.95$ for $S48$, $L/L_0 = 0.88$ for $S74$, and $L/L_0 = 0.82$ of $S100$, all at $P = 0.60\,\text{MPa}$. In the case of $S48$, for increasing input pressures, no change in gauge length is recorded until $P = 0.20\,\text{MPa}$, and the values plateau for $P \geq 0.45\,\text{MPa}$. Secondly, and contrarily to h/h_0, L/L_0 shows a hysteresis extending to higher values of the input pressure as the muscle density increases. This is visible in Fig. 8, where the hysteresis ends at $P = 0.35\,\text{MPa}$ for $S48$, $P = 0.50\,\text{MPa}$ for $S74$ and $P = 0.60\,\text{MPa}$ for $S100$.

It is postulated that the different behaviours derive from the lesser number of weft for a lower muscle density. In $S48$, the warp is not constraining the muscle's expansion, and thus an expansion closer to that of the maximum unwoven muscle's potential is achieved. Moreover, the lesser number of weft of $S48$ compared to $S100$ means the warp remains more in line with the lengthwise axis of the sample. Thus, the longitudinal contraction is minimal. This is confirmed by $S74$ yielding intermediate results. It could, therefore, be hypothesised that $S48$ would yield better tensile properties than $S100$ because the warp will remain better aligned with the direction of the

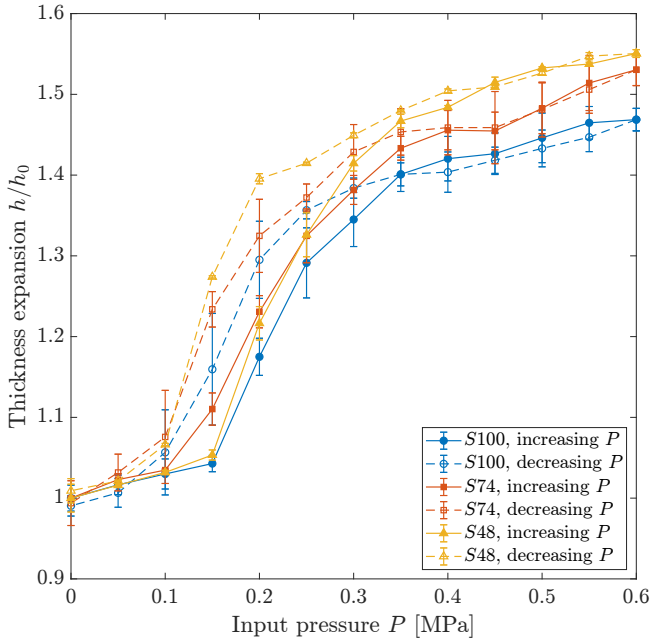

Fig. 7. Thickness expansion h/h_0 of woven samples $S100$, $S74$ and $S48$ for monotonically increasing (solid lines) and monotinically decreasing (dashed lines) pressures ($0.00\,\text{MPa} \leq P \leq 0.60\,\text{MPa}$).

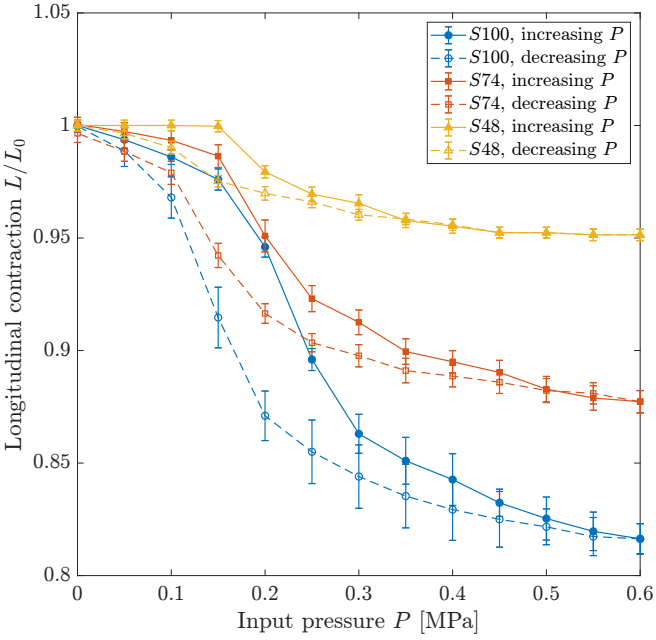

Fig. 8. Longitudinal contraction L/L_0 of woven samples $S100$, $S74$ and $S48$ for monotonically increasing (solid lines) and monotinically decreasing (dashed lines) pressures ($0.00\,\text{MPa} \leq P \leq 0.60\,\text{MPa}$).

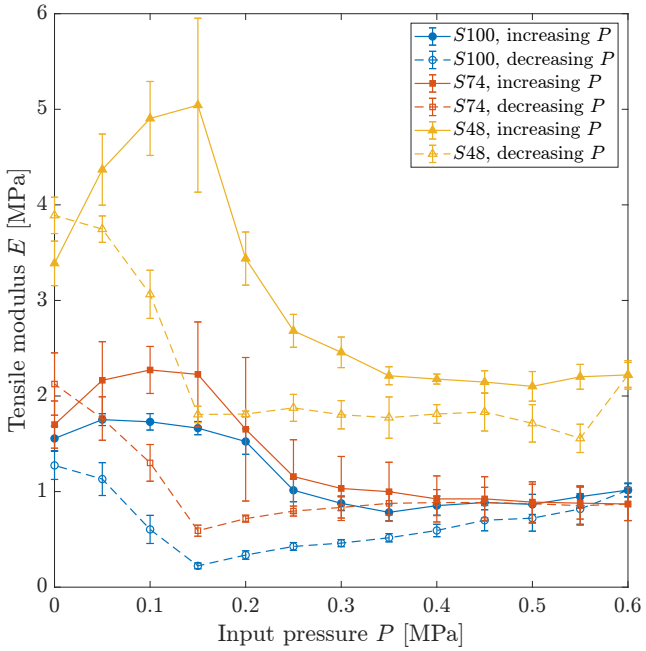

Fig. 9. Tensile modulus E of woven samples samples $S100$, $S74$ and $S48$ for monotonically increasing (solid lines) and monotinically decreasing (dashed lines) pressures ($0.00\,\text{MPa} \leq P \leq 0.60\,\text{MPa}$).

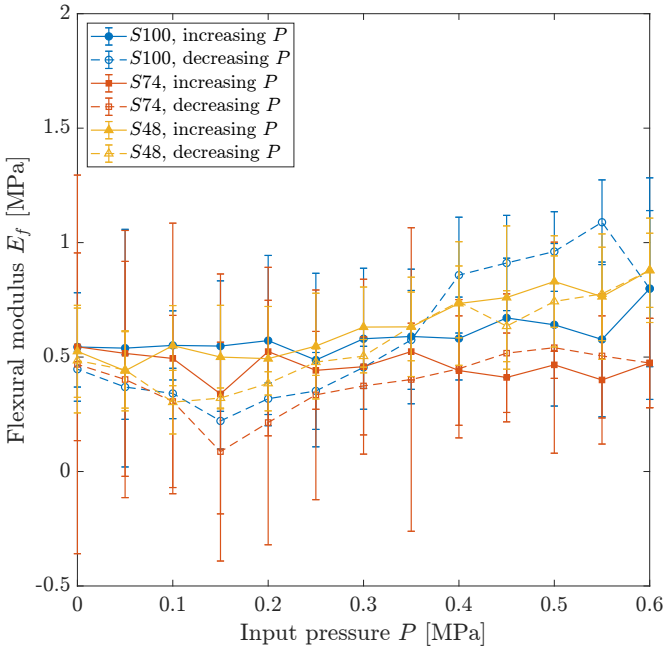

Fig. 10. Flexural modulus E_f of woven samples samples $S100$, $S74$ and $S48$ for monotonically increasing (solid lines) and monotinically decreasing (dashed lines) pressures ($0.00\,\text{MPa} \leq P \leq 0.60\,\text{MPa}$).

tensile load, and $S74$ would display intermediate values of the tensile modulus.

It is also noted that an increasing muscle density yields a higher uncertainty, highlighted by the error bars in Fig. 7 and Fig. 8. This may be relevant to applications where a high degree of reliability and predictability is required.

Here, we have shown that muscle density has a significant impact on the geometrical characterisation of the active textile samples, namely the thickness and length. In Section IV-C and Section IV-D, we endeavour to characterise, for the first time, the effect of muscle density on the mechanical properties of active textiles.

C. Tensile Properties

While previous tensile tests of plain weave pneumatic active textiles have been reported [7], [19], no characterisation of the mechanical properties was undertaken. Fig. 9 presents the tensile modulus of active textiles and its variation with monotonically increasing and monotonically decreasing input pressure at the three muscle densities investigated, namely $\rho_M = 100\,\text{m}^{-1}$, $\rho_M = 74.26\,\text{m}^{-1}$ and $\rho_M = 47.62\,\text{m}^{-1}$. For sample $S48$, the values of E are consistently higher than for $S100$, and closer to the potential of the warp material in isolation. Indeed, experiments conducted on single strands of the nylon 6 warp ($n = 5$) using the methodology presented in Section III yielded a tensile modulus $E = 890.47 \pm 37.47$ MPa. This is because the lesser number of weft in $S48$ compared to $S100$ allows the warp to remain better aligned with the tensile load, and thus exhibit better tensile properties. Sample $S74$, while displaying a tensile modulus between that of $S100$ and $S48$, is closer to that of the former. As such, the results further confirm that E does not vary linearly with ρ_M.

For each muscle density, a local maxima in the value of the tensile modulus is present for increasing P. This is found at $P = 0.05\,\text{MPa}$ for $S100$, $P = 0.10\,\text{MPa}$ for $S74$ and $P = 0.15\,\text{MPa}$ for $S48$. This points at the occurrence of local maxima in association with increasing input pressure as the muscle density decreases. These results bring evidence that the maximum tensile modulus varies with muscle density and input pressure, and that the maximum values of E are achieved for low pressures within the operating range tested in this work.

For decreasing P, all muscle densities display a local minima at $P = 0.15\,\text{MPa}$. At this input pressure, the value of E for decreasing pressure is only 36% of that for increasing pressure for $S48$, 27% for $S74$, and 13% for $S100$. This observation is consistent with a large hysteretic behaviour, in combination with a heavily asymmetric response for the tensile modulus, particularly at $P = 0.15\,\text{MPa}$, where the local maxima for $S48$ occurs for increasing pressure.

The tensile properties of active textiles can, therefore, be altered thanks to a combination of muscle density and input pressure. As tunable stiffness is a key benefit of pneumatic active textile, the flexural modulus is therefore investigated.

D. Flexural Properties

The flexural modulus for all three muscle densities and monotonically increasing and monotonically decreasing input pressures is presented in Fig. 10. An increase in the values of E_f for increasing values of P is apparent for $S100$ and $S48$. Conversely, E_f appears constant for $S74$ for the range of pressures tested. However, it should be noted that the present results are undertaken for a weft orientation perpendicular to the span, i.e. the distance between longitudinal support points

of the 3-point bend test of the samples, see Fig. 4(b). Such orientation dictates that the artificial muscle does not provide a noticeable contribution to the stiffness of the textile, justifying the high uncertainty depicted in Fig. 10.

Consequently, these observations point at the need to better address the effect of weft orientation with respect to the spanwise direction, where the maximum increase in stiffness is expected to occur for a weft aligned with the spanwise direction. This would enable to better assess the flexural modulus over a range of orientations, identify any muscle density effect, and compare experimental results with established theory for off-axis properties of composite materials (e.g. Krenchel factor [27], or classical laminate theory).

Ultimately, these results enable accurate prediction of length L and the thickness h, and in turn of the geometrical properties of the textile sample, despite hysteretic behaviours. Of particular interest is the second moment of area $I = bh^3/12$ about the neutral axis. Indeed, combined with the tensile modulus (Section IV-C), it yields the bending stiffness EI. Moreover, $E_f I$, based on the flexural modulus (Section IV-D) is the flexural rigidity. Both are significant as they allow the prediction of the mechanical behaviour of active textiles, including deflection under operating loads.

V. Discussion

The findings of Section IV provide novel insights into the mechanical properties and behaviour of plain woven active textiles with tunable stiffness and the effect of muscle density for monotonically increasing and monotonically decreasing pressures, namely:

(i) Hysteresis is found to affect the length and diameter of the pneumatic active textiles. This is shown to be independent of muscle types or length. These two factors, however, strongly influence the radial expansion and longitudinal contraction for varying input pressures and will negatively impact actuators' performance during fast duty cycles.

(ii) The three muscle densities tested proved to have a significant impact on the geometrical characterisation of the active textiles under consideration. An increasing muscle density has been associated with a lower thickness expansion, for which the hysteresis extends to a higher input pressure as the muscle density is decreased. Conversely, the longitudinal contraction increases with muscle density, as does the extent of the hysteresis. The greater increase in thickness at a lower muscle density results from the lesser constraints exerted on the muscle by the warp, allowing for an expansion closer to that of the unwoven muscle's maximum potential.

(iii) For increasing input pressures, the tensile modulus is muscle density-dependent, but does not increase linearly with the reduction in muscle density. Indeed, the tensile modulus for $S48$ is far greater than that of $S74$ and $S100$. In all case, there is a local maxima in the value of the modulus, within the range of values tested in this work. The local maxima has been shown to occur at a higher input pressure as the muscle density increases. For increasing pressures, the local maxima and sharp decline in tensile modulus for the subsequent input pressures is associated with the radial expansion of the muscle. Indeed, the decline in tensile modulus coincides with the input pressure at which the increase in thickness expansion of the muscle begins. This results in the warp being deviated from the tensile load axis.

(iv) For decreasing input pressure, the tensile modulus exhibits a vastly different behaviour than for increasing pressures, manifesting significant hysteresis. All muscle densities displayed a local minima at $P = 0.15\,\mathrm{MPa}$. At this pressure the value of the tensile modulus for decreasing pressure compared to increasing pressure is only about one third for $S48$, one quarter of $S74$, and one eighth for $S100$. The results reveal a heavily asymmetrical behaviour when the active textiles are subject to monotonically increasing/decreasing pressures.

(v) The flexural modulus slightly increases with the input pressure for $S48$ and $S100$, while it remains constant for $S74$. These results, however, are affected by a large degree of uncertainty owing to the orientation of the weft being normal to the span during the flexural tests, thus necessitating *ad-hoc* treatment.

VI. Conclusions

Mechanical testing of plain weave pneumatic active textiles was undertaken in tension and flexion employing a nylon 6 warp and thin EM20 McKibben S-muscle weft at three muscle density configurations, namely 100 m^{-1}, 74.26 m^{-1} and 47.62 m^{-1}. The woven active textile was subject to monotonically increasing and monotonically decreasing input pressures ranging from $0.00\,\mathrm{MPa}$ to $0.60\,\mathrm{MPa}$ at $0.05\,\mathrm{MPa}$ increments.

These results offer a clear perspective on the response of this type of active textile to different muscle densities. Importantly, the lower muscle density was associated with larger thickness and smaller length variation of the actuator. Hysteresis was observed consistently and found to be relatable to muscle density, ultimately inducing uneven response of the fabric under increasing or decreasing pressure. This analysis also identifies the interaction between the rubber tube and the outer sleeve of the artificial muscle as the components responsible for the onset of the observed hysteretic behaviour. Muscle orientation under tension and flexion remains an element open to investigation which can guide design choices of the woven pattern to enhance actuator performance.

These novel experimental findings provide a systematic characterization of the fundamental building block of an active fabric, upon which the development of more complex planar and spatial woven patterns can be undertaken. The compliance with established standards used in composite material testing provides confidence in the reliability and reproducibility of the present results, thus facilitating the implementation of this technology in soft robots, wearable technologies, and biomedical devices.

REFERENCES

[1] A. Maziz, A. Concas, A. Khaldi, J. Ståhlhand, N. Persson and E.W.H. Jager, "Knitting and weaving artificial muscles", *Science Advances*, 3:e1600327, 2017.

[2] Y. Chen, Y. Yang, M. Li, E. Chen, W. Mu, R. Fisher and R. Yin, "Wearable actuators: an overview", *MDPI Textiles*, 1, 283–321, 2021.

[3] J. Xiong, J. Chen and P.S. Lee "Functional fibers and fabrics for soft robotics, wearables, and human-robot interface", Advanced Materials, 33, 2002640, 2021.

[4] S. Mun, S. Yun, S. Nam, S.K. Park, S. Park, B.J. Park, J.M. Lim and K.U. Kyung, "Electro-active polymer based soft tactile interface for wearable devices", IEEE Transactions on Haptics, 11, 15–21, 2018.

[5] J. Hu, H. Meng, G. Li ans S.I. Ibekwe, "A review of stimuli-responsive polymers for smart textile applications", Smart Materials and Structures, 21, 053001, 2012.

[6] S. Kurumaya, H. Nabae, G. Endo, and K. Suzumori. "Design of thin McKibben muscle and multifilament structure". *Sensors and Actuators A: Physical*, 261: 66-74, 2017.

[7] T. Hiramitsu, K. Suzumori, H. Nabae, and G. Endo. "Experimental evaluation of textile mechanisms made of artificial muscles." *2nd IEEE International Conference on Soft Robotics (RoboSoft)*, pp. 1-6, 2019.

[8] R. Younes, K. Hines, J. Forsyth, J. Dennis, T. Martin, M. Jones, "The design of smart garments for motion capture and activity classification",in Woodhead Publishing Series in Textiles, Smart Textiles and their Applications, 627-655, 2016.

[9] M. ten Bhömer, O. Tomico, S. Wensveen, "Designing ultra-personalised embodied smart textile services for well-being", in Woodhead Publishing Series in Textiles, Advances in Smart Medical Textiles, 155-175, 2016.

[10] M. Zhu, T.N. Do, E. Hawkes, Y. Visell, "Fluidic fabric muscle sheets for wearable and soft robotics", Soft Robotics, 7(2), 179-197, 2020.

[11] C.T. O'Neill, C.M. McCann, C.J. Hohimer, K. Bertoldi, C.J. Walsh, "Unfolding textile-based pneumatic actuators for wearable applications", Soft Robotics, 9(1), 163-172, 2022.

[12] R. Andreasson, B. Alenljung, E. Billing, R. Lowe, "Affective touch in human–robot interaction: conveying emotion to the Nao robot", *International Journal of Social Robotics*, 10. pp 473-491, 2018.

[13] S. Yohanan, K. E. MacLean, "The role of affective touch in human-robot interaction: human intent and expectations in touching the haptic creature", *International Journal of Social Robotics*, 4. pp 163-180, 2012.

[14] A. Haynes, A. Lywood, E. Crowe, J. L. Fielding, J. M. Rossiter, C. Kent, "A calming hug: design and validation of a tactile aid to ease anxiety", *PLoS ONE*, 2022, 17(3), [e0259838]. https://doi.org/10.1371/journal.pone.0259838

[15] E. Pulvirenti, R. S. Diteesawat, H. Hauser and J. Rossiter, "Towards a soft exosuit for hypogravity adaptation: design and control of lightweight bubble artificial muscles", *2022 IEEE 5th International Conference on Soft Robotics (RoboSoft)*, Edinburgh, United Kingdom, 2022, pp. 651-656.

[16] R. S. Diteesawat et al., "A Soft Fabric-based Shrink-to-fit Pneumatic Sleeve for Comfortable Limb Assistance," *2022 IEEE/RSJ International Conference on Intelligent Robots and Systems (IROS)*, Kyoto, Japan, 2022, pp. 9766-9773.

[17] E. T. Roche, M. A. Horvath, I. Wamala, A. Alazmani, S. Song, W. Whyte, Z. Machaidze, C. J. Payne, J. C. Weaver, G. Fishbein, J. Kuebler, N. V. Vasilyev, D. J. Mooney, F. A. Pigula, C. J. Walsh, "Soft robotic sleeve supports heart function", *Science Translational Medicine*, 9. 373, eaaf3925, 2017.

[18] V. Sanchez, C. J. Walsh, and R. J. Wood. "Textile technology for soft robotic and autonomous garments". *Advanced Functional Materials* 31:2008278, 2020.

[19] A. Ohno, Y. Yamamoto, M. Oguro, and K. Suzumori. "Comparison in characteristics of textile Woven by thin pneumatic artificial muscle". *International Conference on Advanced Mechatronics: Toward Evolutionary Fusion of IT and Mechatronics: ICAM*, pp. 43-44, 2015.

[20] I. Must, E. Sinibaldi, and B. Mazzolai. "A variable-stiffness tendril-like soft robot based on reversible osmotic actuation". *Nature Communications* 10:344, 2019.

[21] E. G. Hocking, and N. M. Wereley. "Analysis of nonlinear elastic behavior in miniature pneumatic artificial muscles". *Smart Materials and Structures* 22:014016, 2013.

[22] International Organization for Standardization. *"ISO 178:2019 Plastics - Determination of flexural properties"*. International Organization for Standardization, Geneva, Switzerland, 2019.

[23] International Organization for Standardization. *"ISO 527-2:2012 Plastics - Determination of tensile properties - Part 2: Test conditions for moulding and extrusion plastics"*. International Organization for Standardization, Geneva, Switzerland, 2012.

[24] International Organization for Standardization. *"ISO 13934-1:2013 Textiles - Tensile properties of fabrics - Part 1: Determination of maximum force and elongation at maximum force using the strip method"*. International Organization for Standardization, Geneva, Switzerland, 2013.

[25] H. W. Coleman, and W. G. Steele. "Engineering application of experimental uncertainty analysis". *AIIA Journal*, 33(10): 1888-1896, 1995.

[26] J.-B R. G. Souppez, and J. Laci. "Ultimate strength of quasi-isotropic composites: ISO 12215-5:2019 validation." *The Royal Institution of Naval Architects Part A: International Journal of Marine Engineering*, 162(A), 237-246, 2022.

[27] H. Krenchel. *"Fibre reinforcement; theoretical and practical investigations of the elasticity and strength of fibre-reinforced materials"*. 1st ed, Akademisk forlag, Copenhagen, 1964.